Journal of Power Sources 267 (2014) 553–559

Contents lists available at ScienceDirect

Journal of Power Sources

journal homepage: www.elsevier.com/locate/jpowsour

Monothioanthraquinone as an organic active material for greener lithium batteries

Adriana Iordache [a, b], Vincent Maurel [b], Jean-Marie Mouesca [b], Jacques Pécaut [b], Lionel Dubois [b, *], Thibaut Gutel [a, *]

[a] CEA, LITEN (DRT/LITEN/DEHT/LMB), Laboratoire des Matériaux pour Batteries, 17 rue des martyrs, F-38054 Grenoble, France
[b] CEA, INAC (DSM/INAC/SCIB), UMR-E CEA-UJF, Laboratoire de Chimie Inorganique et Biologique, 17 rue des martyrs, F-38054 Grenoble, France

HIGHLIGHTS

- Thioquinone as active material for lithium ion batteries.
- Thiocarbonyl function shifts the potential towards more positive values.
- Thioquinone cyclability is improved compared with quinone.

GRAPHICAL ABSTRACT

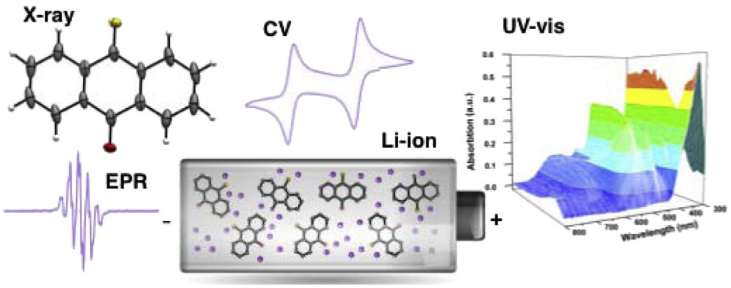

ARTICLE INFO

Article history:
Received 20 February 2014
Received in revised form
25 April 2014
Accepted 7 May 2014
Available online 20 May 2014

Keywords:
Lithium-ion
Organic batteries
Monothioanthraquinone
Electrochemistry

ABSTRACT

In order to reduce the environmental impact of human activities especially transportation and portable electronics, a more sustainable way is required to produce and store electrical energy. Actually lithium battery is one of the most promising solutions for energy storage. Unfortunately this technology is based on the use of transition metal-based active materials for electrodes which are rare, expensive, extracted by mining, can be toxic and hard to recycle. Organic materials are an interesting alternative to replace inorganic counterparts due to their high electrochemical performances and the possibility to produce them from renewable resources. A quinone derivative is synthetized and investigated as novel active material for rechargeable lithium ion batteries which shows higher performances.

1. Introduction

Compared with conventional inorganic materials, organic compounds for electrode materials of lithium batteries present better electrochemical performances such as high theoretical specific capacity and tunable redox potential due to easy structure design. They also offer the opportunity to develop low cost and sustainable batteries thanks to the abundance of raw materials and their low environmental footprint. The concept of organic electrode materials itself is not new. For example, dichloroisocyanuric acid was reported as a cathode material for primary Li batteries in 1969 [1]. Conducting polymers such as polyacetylene, polyaniline, polythiophene, polypyrrole and their derivatives have also been utilized as organic cathode materials [2]. However, these materials have attracted much less attention than their inorganic counterparts.

Recently published reviews have shown significant progress in the incorporation of organic materials based on radical and

* Corresponding authors.
E-mail addresses: lionel.dubois@cea.fr (L. Dubois), thibaut.gutel@cea.fr (T. Gutel).

http://dx.doi.org/10.1016/j.jpowsour.2014.05.050
0378-7753/

carbonyl groups such as anhydride and quinone structures in rechargeable Li batteries [3].

Quinones are attractive materials involving two electron transfers in two well-separated processes: the first electron transfer is assigned to radical anion formation and the second to dianion formation accompanied by two consecutive Li^+ association. Previous investigations [4] show that quinones have good redox performances and electrochemical reversibility. Furthermore, some of the quinones can eventually be produced directly from biomass [5–7]. Therefore, quinone compounds are promising energy storage materials. However, the fact should not be ignored that quinone materials have several disadvantages in terms of their electrical insulation and significant solubility in electrolytes.

In the past years, anthraquinone (AQ) has been extensively studied as an active material for electrodes of Li-ion batteries either as small molecules [8–14] or in their polymeric form [15–18]. Recently, Liang et al. [19] reported anthraquinone analogues incorporating fused heteroaromatic structures as cathode materials in rechargeable lithium batteries. They showed that rational incorporation of heteroatoms improves the cell performances.

In our work, the strategy was to replace the carbonyl groups of the anthraquinone with thiocarbonyl, giving rise to monothioanthraquinone or dithioanthraquinone. In this paper, we report on the use of monothioanthraquinone as an improved positive material regarding the cell performances in terms of specific gravimetric capacity, working potential, and cyclability.

The synthesis of monothioanthraquinone (MTAQ) was first described in the early '80 by Raasch [20]. In contrast to monothioanthraquinone, the dithioquinones are highly reactive making their handling and isolation in pure form a difficult task. Thus, examples of dithioquinones are scarce, [21–24] dithio-*para*-benzoquinone has only been generated and characterized spectroscopically at low temperature (10 K) in argon matrix [24]. Cava and coworkers [23] attempted to synthesize dithioanthraquinone using two pathways: direct thionation of anthraquinone or monothioanthraquinone and thionation of a monothioanthraquinone-2,3-dimethylbutadiene adduct followed by retro-Diels–Alder reaction. Both strategies systematically lead to a red polymeric material. Their results clearly demonstrate that the dithioanthraquinone is inherently reactive in contrast to monothioanthraquinone and tends to polymerize into polydisulfides. Since our goal was to study the influence of thiocarbonyl groups on the cell performances, no dithioanthraquinone analogue was synthetized, only the monothioanthraquinone was further investigated as active material for Li-ion batteries.

2. Experimental section

2.1. Synthesis and characterization

All chemicals were used as received unless otherwise noted. Anthrone (97%), anthraquinone (97%) were purchased from Aldrich. Anhydrous ethanol and DMF were purchased from Carlo Erba and Aldrich, respectively. Monothioanthraquinone synthesis has been achieved starting from the commercially available anthrone with an overall yield of 50% and following published procedures [20,25]. MTAQ and intermediates were characterized by NMR, IR, SM and UV–vis spectroscopy (See SI). The AQ was purified by recrystallization in chloroform.

^1H NMR and ^{13}C NMR spectra were recorded on Bruker 200 MHz spectrometer. ^1H chemical shifts (ppm) were referenced to residual solvent peaks. UV–vis–NIR spectra were recorded on a lambda 950 spectrophotometer (Perkin Elmer) using conventional quartz cells (Hellma Inc.). FTIR measurements were realized using a Thermo Scientific Nicolet 6700 spectrometer.

2.2. Electrode preparation and cell test

Coin cells for battery tests were prepared in an Ar filled glove box as follow. A working electrode was first prepared by mixing AQ or MTAQ powder, Super P® (TimCal) as conductive additive, and polyvinyldifluoride (PvdF, 12% solution in *N*-methyl-2-pyrrolidone or NMP) as the binder in a weight ratio of 40:40:20. The slurry was coated to an aluminium foil current collector, and the resulting positive electrode was dried for 48 h at 60 °C under vacuum. The prepared positive electrode and a lithium metal foil negative electrode were assembled in coin cells with a Celgard® 2400 (Celgard) and Viledon® (Freudenberg) as separators. The electrolyte was a mixture of ethylene carbonate (EC), dimethyl carbonate (DMC), ethyl methyl carbonate (EMC) (EC:DMC:EMC = 1:1:1) and 1 M $LiPF_6$ (UBE).

2.3. Electrochemistry and spectroelectrochemistry

Cyclic voltammetry (CV) was recorded using a Biologic potentiostat (SP 300). All analytical experiments were conducted under an argon atmosphere (glove box) in a standard one-compartment, three-electrode electrochemical cell. Tetra-*n*-butylammonium hexafluorophosphate ($TBAPF_6$) was used as supporting electrolyte (0.1 M) in acetonitrile (AN) or lithium hexafluorophosphate (1 M $LiPF_6$) in mixture of ethylene carbonate (EC), dimethyl carbonate (DMC), ethyl methyl carbonate (EMC) in a 1:1:1 ratio. Glassy carbon (Ø = 3 mm) based working electrode was polished with diamond paste (0.1 μm) before each recording. All CVs were recorded using an Ag/AgCl reference electrode and ferrocene as internal reference. All spectroelectrochemical measurements were recorded using a freshly prepared Ag/Ag^+ reference electrode (0.01 M $AgNO_3$ in 0.1 M $TBAPF_6$/AN). All potentials were converted using the relation $E_{1/2}^{Fc/Fc+}$ = 3.25 V *vs.* Li^0/Li^+, which was measured in a mixture of EC:DMC:EMC = 1:1:1 (1 M $LiPF_6$). All potentials are given *vs.* Li^+/Li^0. Anhydrous AN and $TBAPF_6$ (99%, electrochemical grade) were purchased from Aldrich and used without further purification. Spectroelectrochemical measurements were carried out in a glove box with a standard potentiostat (OrigaLys) coupled to a Shimadzu 2600 spectrophotometer using 0.5 cm stainless steel immersion probe.

2.4. EPR and DFT calculations

EPR spectra were recorded using a Bruker EMX spectrometer equipped with a rectangular cavity. Due to the use of acetonitrile as a solvent in the samples to be studied, 20 μL of the electrolysis solution were introduced in a glass capillary tube of ~1 mm internal diameter and the capillary tube was enclosed in a regular EPR tube (4 mm external diameter) under argon atmosphere. Typical EPR parameters for these measurements were: Sweep width = 25 G, Center Field = 3431.5 G, resolution = 1024 points, Frequency = 9.6589 GHz, Microwave Power = 2.0 mW, Receiver Gain = 4.0E5, Modulation amplitude = 0.15 G, Conversion time = 80 ms; Time Constant = 20 ms. Number of scans = 14. The numerical simulation of EPR spectra was performed using Easyspin package 4.5.1 [26].

Hyperfine coupling constants and the g-tensor have been computed by Density Functional Theory (DFT) using the ADF package (2012) [27] with the standard hybrid B3LYP exchange–correlation (XC) potential [28,29]. We used a triplet-ζ basis set for all atoms (no frozen-core option). Before that, geometry optimizations have been performed with the same hybrid XC potential in the presence of a dielectric continuum modelled with the ADF-COSMO (COnductor-like Screening MOdel) [30–32] module (ε = 37). Hyperfine coupling constants turned out to be sensitive to

slight geometrical changes induced by the presence/absence of this dielectric environment. Best results (i.e. better correlation) were obtained in its presence. UV–vis absorption spectra were calculated with the ADF time-dependent DFT (TD-DFT) module using standard procedures (Davidson's algorithm) [33,34]. We relied on the SAOP (Statistical Average Of Potential) exchange-potential, [35] specifically designed to exhibit the proper $(-1/r)$ asymptotic behaviour outside the molecular model. Finally, five molecular orbitals have been separately computed using the ORCA package (version 2.6) developed by Franck Neese's group, now at the Max-Planck Institute für Chemische Energie Konversion (available free of charge from the ORCA's website cec.mpg.de).

2.5. Crystallography

Diffraction data were taken using an Oxford-Diffraction XCallibur S kappa geometry diffractometer (Mo-Kα radiation, graphite monochromator, $\lambda = 0.71073$ Å). The data were collected at 150 K. The cell parameters were obtained with intensities detected on three batches of 5 frames. The crystal-detector distance was 4.5 cm. 750 narrow data were collected with CrysAlisPro Oxford-diffraction software with 1° increments in ω with an exposure time of 80 s. The substantial redundancy in data allows empirical absorption corrections to be applied using multiple measurements of equivalent reflections. Space groups were determined from systematic absences, and they were confirmed by the successful solution of the structure. The structures were solved by flipping charge methods using the superflip software, [36] refine with Olex2-1.2ac2 package [37]. All atoms were found by difference Fourier syntheses. All non-hydrogen atoms were anisotropically refined whereas hydrogen atoms remains isotropic.

CrysAlisPro Version 1.171.33.34d: Agilent (2010). CrysAlis PRO. Agilent Technologies, Yarnton, England. SHELXTL Version 6.14: Sheldrick, G. M. (1997). Bruker AXS Inc., Madison, Wisconsin, USA.

CCDC 978799 contains the supplementary crystallographic data for this paper. These data can be obtained free of charge from The Cambridge Crystallographic Data Centre via www.ccdc.cam.ac.uk/data_request/cif.

3. Results and discussion

3.1. Synthesis and crystal structure

The MTAQ was synthetized as described in the literature and fully characterized (Figs. S1–S5). Green needles-like single crystals of MTAQ were obtained by sublimation under Ar flow at 200 °C. The Ortep [38] views (50% probability) and crystal data can be found in the supplementary information (Fig. S6 and Table S1) and show a coplanar arrangement of the MTAQ rings. The crystal structure displays stacking of MTAQ by π–π interactions to form column structures as shown in Fig. S6b. In the columns the mean intermolecular distances are 3.45 Å. The position of the carbonyl and thiocarbonyl are interconverted (randomly or alternatively) in the crystal, so for a given position, each atom (S or O) possess an occupancy coefficient of 0.5.

3.2. Charging/discharging behaviours and cycle-life stabilities

The electrochemical activity of AQ and MTAQ was first studied by cyclic voltammetry (CV) in a coin cell battery using mixture of EC:DMC:EMC = 1:1:1 (1 M $LiPF_6$) as electrolyte. The CV curves performed with electrode containing 40% AQ or MTAQ, 40% SuperP® and 20% binder (% wt) are shown in Fig. 1. This electrode composition is suitable for the organic active materials due to their low electronic conductivities. In the following all potentials are given *vs.* Li^+/Li^0. It can be seen from Fig. 1a that AQ shows two reduction processes associated with two Li^+ complexation at around 2.15 and 2.09 V which correspond to the electrogeneration of mono- ($AQLi^•$) and di-lithium ($AQLi_2$) salts (Scheme 1a). In the reverse scan just one oxidation process was found at 2.47 V assigned to the re-oxidation of $AQLi_2$ followed by two Li^+ dissociations. These results are in complete agreement with the electrochemical data published in the literature [8].

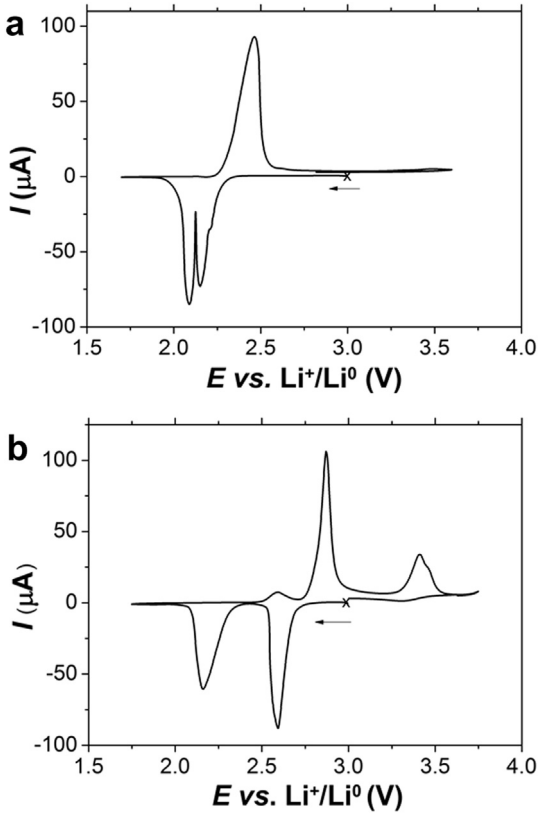

Fig. 1. CV curves performed on coin cells using electrodes of a) AQ and b) MTAQ. AQ or MTAQ/SuperP/Binder = 40/40/20 (% wt) using lithium metal as counter/negative electrode in 1 M $LiPF_6$/EC:DMC:EMC = 1:1:1. $E^{Fc/Fc+}_{1/2} = 3.25$ V *vs.* Li^+/Li^0 in 1 M. $LiPF_6$/EC:DMC:EMC = 1:1:1 [45]. Fc/Fc^+ = ferrocene/ferricinium. Binder = 12% PvdF in *N*-methyl-2-pyrrolidone (NMP).

The first reduction process of MTAQ and the complexation of one Li^+ at 2.59 V takes place at a higher potential than the AQ (Fig. 1b). This shift in potential is in agreement with the introduction of a less electronegative atom, sulphur compared to oxygen,

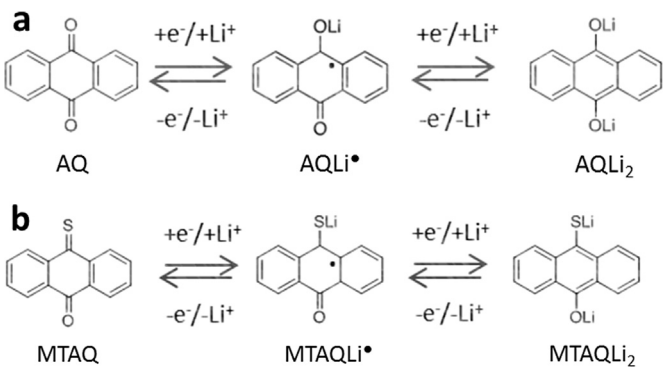

Scheme 1. Schematic diagram of the proposed Li-ion complex formation/2 step redox reaction of a) AQ and b) MTAQ.

suggesting that this process correlates with the transformation of thiocarbonyl group to the lithium thiolate accompanied with the complexation of one Li^+ (Scheme 1b). The second reduction process noticed at 2.16 V matches with the mono-electronic reduction of the carbonyl group in order to electrogenerate the dilithiated salt ($MTAQLi_2$). In the reverse scan, three oxidation peaks are found at 2.59, 2.87, and 3.41 V respectively. The oxidation process observed at 2.87 V involves a major contribution of the dissociation of Li^+ from the thiolate group. If the process is limited to the one electron reduction of MTAQ into $MTAQLi^{\bullet}$ (Fig. S7), the expected re-oxidation process is slightly changed in term of current intensity and shape of the wave. The two oxidation processes at 2.59 and 3.41 V are undoubtedly associated to the second reduction process, the carbonyl reduction ($MTAQLi^{\bullet}$) to the di-lithium salt ($MTAQLi_2$) accompanied by the complexation of one Li cation. These processes could be the result of the dissolution of the active material (MTAQ), and/or of the electrogenerated intermediates ($MTAQLi^{\bullet}$ and $MTAQLi_2$) or of new electrogenerated compounds from potentially side reactions.

The charge/discharge behaviours of AQ and MTAQ as positive electrodes are illustrated in Fig. 2. Fig. 2a shows the typical profile of AQ material, [8] with a plateau at around 2.2 V during the discharge process. The observed discharge capacity of 214 mAh g^{-1} represents 83% of the theoretical value (257 mAh g^{-1}) and corresponds to a two-electron reduction process of AQ. The MTAQ material shows at the first discharge cycle two well-defined plateaus at around 2.7 and 2.1 V respectively (Fig. 2b), perfectly matching with the first and the second reduction processes observed in the CV curve of the electrode made from the MTAQ (Fig. 1b). The first charge cycle of MTAQ electrode displays two major plateaus at around 2.8 and 3.4 V respectively, and a small plateau at around 2.6 V comparable with the three oxidation processes found in Fig. 1b. Despite an initial specific capacity of about 222 mAh g^{-1}, which is close to the nominal value of 239 mAh g^{-1}, a reduction of the observed capacity starts at the second discharge cycle followed by the emerging of new plateaus.

The cycling performances of the electrodes made with AQ and MTAQ are displayed in Fig. 3. The capacity of AQ electrode decreases to ~10 mAh g^{-1} over 40 cycles. The capacity decay measured for the MTAQ electrode shows a rapid decrease for the first four cycles which is stabilized at around 75 mAh g^{-1} over the next 40 cycles. The reasons for this decrease of capacity can be the dissolution of redox active molecules into the electrolyte and/or the potentially side reactions.

3.3. Electrochemical measurements in solution

In order to better understand the electrochemical behaviour of the AQ and MTAQ observed in coin cells, we decided to investigate these compounds by cyclic voltammetry, spectroelectrochemistry, EPR studies in solution and DFT calculations.

3.3.1. Cyclic voltammetry

The electrochemical activity of AQ and MTAQ has been studied in 0.1 M $TBAPF_6$/AN and in 1 M $LiPF_6$/EC:DMC:EMC = 1:1:1. The CV curves of AQ and MTAQ in 0.1 M $TBAPF_6$/AN (Fig. 4a) exhibit similar patterns showing both well-known consecutive reversible reductions: the first electron transfer is assigned to radical anion formation (at 1.96 for AQ and 2.53 V for MTAQ) and the second to dianion formation (at 1.42 for AQ and 1.84 V for MTAQ) (Scheme 1). The insertion of a softer atom sulphur instead oxygen is inducing a decrease in energy of the HOMO orbital, corresponding to the MTAQ irreversible oxidation process at 4.53 V assigned as the radical cation generation. As expected, the thiocarbonyl has an important effect on the first reduction processes of MTAQ with higher potential observed (Table 1). The positive shift of 0.57 V for the first reduction process is also in agreement with the introduction of a less electronegative atom sulphur compared with oxygen. This first process can therefore be assigned as the reduction of the thiocarbonyl group C=S (Scheme 1b).

The CV curves of AQ and MTAQ recorded in a mixture of EC:DMC:EMC = 1:1:1 (1 M $LiPF_6$) show different shapes suggesting different kinetics (Fig. 4b). Cations present in the supporting electrolyte interact with the electrogenerated radical anions and dianions, the level of their association depending on the identity of both ions and the employed solvent. In the presence of tetraalkylammonium cations in aprotic solvents, for example, the degree of ion pairing is often assumed small enough to be negligible and, hence, their widespread use in electrolyte solutions. However, alkali metal cations have a tendency to form complexes with organic anions, which can have a dramatic effect on the observed

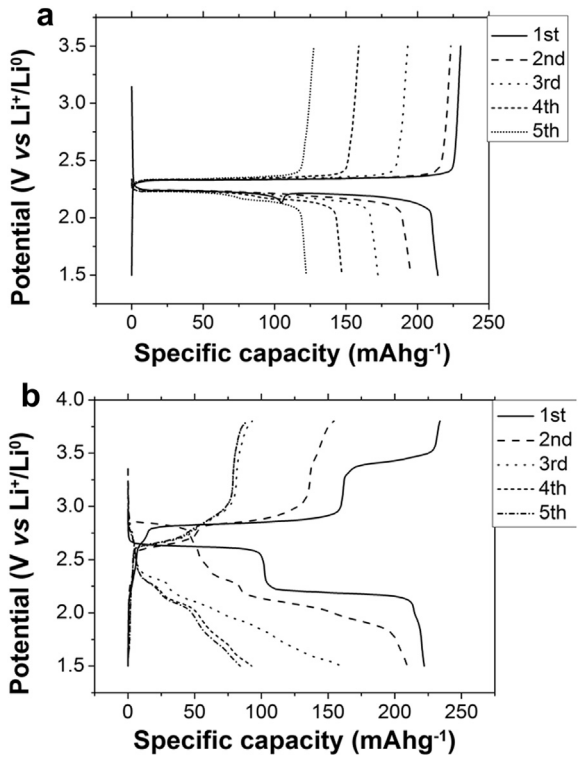

Fig. 2. Firsts five cycles of lithium half cells using a) AQ and b) MTAQ as cathode material cycled at C/10. AQ or MTAQ/SuperP/Binder = 40/40/20 in 1 M $LiPF_6$/EC:DMC:EMC = 1:1:1.

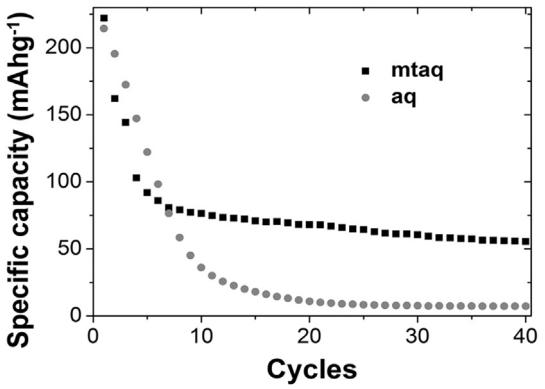

Fig. 3. Cycle-life performances of the prepared electrodes AQ and MTAQ at C/10 rate.

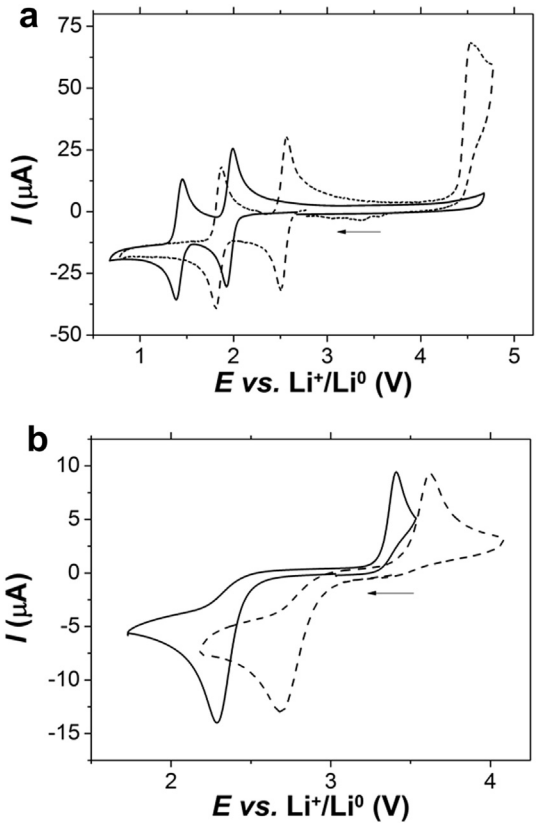

Fig. 4. CV curves of AQ (solid line) and MTAQ (dashed line) in a) 0.1 M $TBAPF_6$/AN and b) 1 M $LiPF_6$/EC:DMC:EMC = 1:1:1, 3 mm glassy carbon, 298 K, $\nu = 0.1$ V s^{-1}, *E vs.* Li^0/Li^+.

voltammetry and is manifested in the shifting of voltammetric reduction peaks to higher potentials as the anions are thermodynamically stabilized by the ion pairing interaction. The extent of this has been found to increase as the cationic radius decreases, suggesting that complex formation is most significant with the Li^+ [39]. Therefore, the reduction processes of AQ and MTAQ, at 2.29 and respectively at 2.69 V represent an overall two-electron reduction processes in order to finally generate the dilithiated salts $AQLi_2$ and respectively $MTAQLi_2$. At the reverse scan rate, the re-oxidation processes of the electrogenerated salts are detected (3.41 and respectively 3.62 V). The irreversible oxidation process of MTAQ in 1 M $LiPF_6$ and EC:DMC:EMC = 1:1:1 observed at 4.5 V is shown in Fig. S8. Since the surfaces of the reduction and the corresponding re-oxidation waves are not equivalent, we suspect also some adsorption/desorption phenomena at the working electrode interface due to the low solubility of the lithiated species.

3.3.2. Spectroelectrochemistry, EPR studies and DFT calculations

In-situ spectroelectrochemical analyses were carried out to obtain further insight into the nature of the electrogenerated species. For these investigations, absorption spectra were recorded periodically as the AQ (Fig. 5a) and MTAQ (Fig. 5b) were submitted to bulk electrolyses. Electrochemical reductions of AQ and MTAQ (up to one electron per molecule, Fig. 5 and up to two electrons per molecule, Fig. S9 were performed in 0.1 M $TBAPF_6$ and anhydrous acetonitrile as electrolyte. Bulk electrolyses of AQ and MTAQ were attempted using a mixture of 0.1 M $LiPF_6$ and EC:DMC:EMC = 1:1:1, but the new electrogenerated species were adsorbed at the electrode surface leading to electrode passivation.

Reduction of AQ in the potentiostatic regime upon setting the potential of a platinum working electrode at 1.84 V *vs.* Li^+/Li^0, produced an absorption loss of the $\pi \rightarrow \pi^*$ transition at ~320 nm and the appearance of new spectroscopic patterns with the absorption band at λ = 390 and 410 nm (ε = 4400 M^{-1} cm^{-1}), at 545 nm (ε = 9600 M^{-1} cm^{-1}) with a shoulder at 510 nm and at ~800 nm (Fig. 5a). The colour changes from very pale yellow to red-pink. This signature is typical for monoradical anion $AQ^{\bullet-}$ [40–42]. The reversibility of the reduction process at the electrolysis time scale was also followed by UV–vis absorption spectroscopy which showed the recovery of the initial species after back electron transfer. The spectroscopic prints of the dianion AQ^{2-} were resolved by two-electron reduction of AQ by applying a working potential of 1.04 V *vs.* Li^+/Li^0 (Fig. S9a). At the first stage of the reduction process (solid arrows) the specific absorption bands of $AQ^{\bullet-}$ appear followed by their decrease in intensity at the expense of new signals growing at ~500 and 700 nm (dashed arrows) characteristic for the AQ^{2-}.

The exhaustive one electron reduction of the MTAQ at 2.24 V led to significant changes in its absorption spectra (Fig. 5b); showing the decrease of the $\pi \rightarrow \pi^*$ absorption band at 330 nm

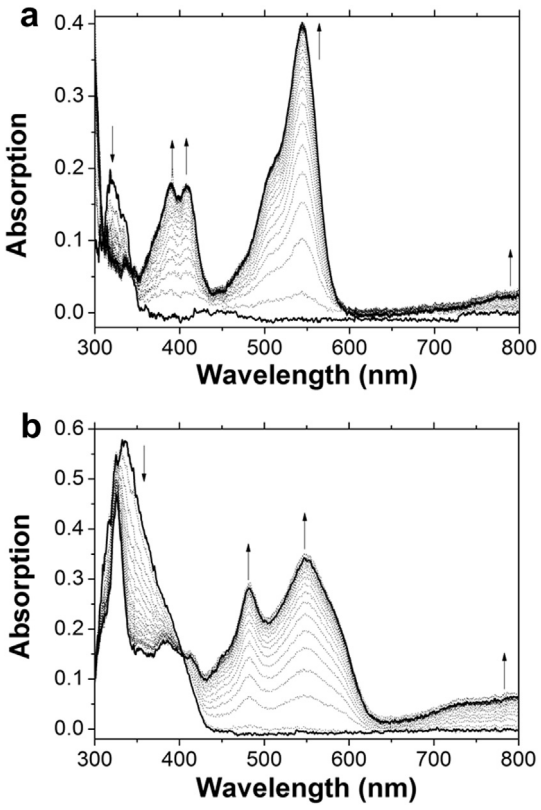

Fig. 5. UV–vis spectra recorded with an optical path of l = 0.5 mm during the exhaustive one-electron reduction of (a) AQ and (b) MTAQ. 0.08 mM in AN (0.1 M $TBAPF_6$) using a platinum plate working electrode whose potential was fixed at E_{ap} = 1.84 and 2.24 V *vs.* Li^+/Li^0 respectively.

Table 1
Electrochemical data[a,b] of AQ and MTAQ.

Compound	$E^1_{1/2}$,[a] V	ΔE^1_p,[a] mV	$E^2_{1/2}$,[a] V	E_{pa},[a] V	E_{pc},[b] V	E_{pa},[b] V
AQ	1.96	60	1.42	–	2.29	3.41
MTAQ	2.53	60	1.84	4.53	2.69	3.62

[a] 0.1 M $TBAPF_6$/AN.
[b] 1 M $LiPF_6$/EC:DMC:EMC = 1:1:1, glassy carbon 3 mm, 298 K, $\nu = 0.1$ V s^{-1}. $E_{1/2} = (E_{pa} + E_{pc})/2$. $\Delta E_p = |E_{pa} - E_{pc}|$ are measured at $\nu = 0.02$ V s^{-1}. $E^{Fc/Fc^+}_{1/2} = 3.25$ V *vs.* Li^+/Li^0 in EC:DMC:EMC = 1:1:1 (1 M $LiPF_6$) [45].

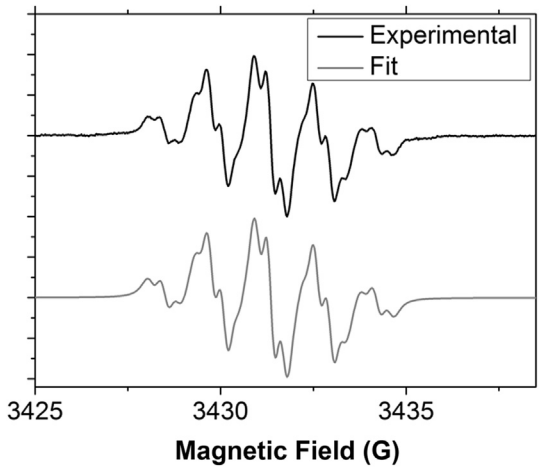

Fig. 6. X-band EPR spectra of MTAQ (experimental: top and fitted: bottom) recorded at 298 K, 0.08 mM in 0.1 M $TBAPF_6$ and AN.

(ε = 13,700 M^{-1} cm^{-1}) becoming sharper and shifted toward the blue region (325 nm, ε = 11,000 M^{-1} cm^{-1}) and the growth of signals in the visible range at 480 nm (ε = 6800 M^{-1} cm^{-1}), 550 nm (ε = 8200 M^{-1} cm^{-1}) and NIR range at 800 nm (Fig. 2b). These changes are thus easily attributed to the simple and clean transformation of MTAQ into $MTAQ^{\bullet-}$, proceeding via a well-defined isosbestic point at 403 nm (Fig. 5b). The spectroscopic prints of the $MTAQ^{\bullet-}$ are slightly different compared to the $AQ^{\bullet-}$, the tween signals at 390 and 410 nm recorded for the $AQ^{\bullet-}$ may be hidden by the transitions between 300 and 450 nm for the $MTAQ^{\bullet-}$ and the intense absorption band at 545 nm splits in two new signals at 480 and 550 nm respectively. Given the difference expected for the electronegativity of oxygen and sulphur, this new signature may suggest that in the case of $MTAQ^{\bullet-}$ the unpaired electron is centred on the sulphur atom. Photochemical studies realized by Natarajan et al. [43] in benzene support the same assumption. This hypothesis was confirmed by EPR studies (see discussion below). The two-electron electrolysis of MTAQ at 1.54 V *vs.* Li^+/Li^0 gives rise to the spectroscopic response of the $MTAQ^{\bullet-}$ (Fig. S9b, solid arrows) which gradually evolve into the dianion $MTAQ^{2-}$ (dashed arrows) characterized by new absorption bands at 385 nm (ε = 7000 M^{-1} cm^{-1}), 460 nm (ε = 9000 M^{-1} cm^{-1}), 530 nm (ε = 3500 M^{-1} cm^{-1}) and a broad signal at 625 nm (ε = 3000 M^{-1} cm^{-1}). The colour of the solution gradually changed from a green pale colour to red-pink and finally to a dark green colour.

The radical anion generation MTAQ was further confirmed upon analysing samples of the electrolyzed solutions by EPR spectroscopy (Fig. 6). The latter was collected at room temperature after ~30% electrochemical reduction of MTAQ (E_{ap} = 2.24 V). This EPR spectrum was numerically fitted with the spectrum of a free radical containing three pairs of two equivalent protons (4.5 MHz, 3.55 MHz, 0.95 MHz) (Fig. 6) and a *g* value of 2.0100. Such EPR spectral features are consistent with the EPR spectrum of the monoanion free radical of MTAQ generated by electrolysis in dimethylsulfoxide reported by Alberti et al. (see Table 2) [44].

Table 2
Experimental and computed EPR parameters of the $MTAQ^{\bullet-}$ free radical.

	aH2,7 (MHz)	aH4,5 (MHz)	aH3,6 (MHz)	aH1,8 (MHz)	*g*
Experimental	4.49 ± 0.2	3.57 ± 0.2	0.95 ± 0.1	–	2.0100
Alberti et al. [44]	4.36	3.46	0.90	–	2.0099
DFT	−4.9	−4.1	+1.1	(+0.6)	2.0105

Furthermore hyperfine splitting constants and *g* value of this free radical were computed by DFT calculations (Table 2) and the computed values are in good agreement with experimental values.

Spectra recorded for longer times of electrolysis (data not shown) were similar and could be attributed to the same free radical, but, rather unexpectedly, they did not showed a significant increase in the EPR signal. However the EPR spectrum of the sample described in Fig. 6 decayed slowly (55% decay after 3 h at room temperature) indicating that the mono-anion free radical of monothioanthraquinone is relatively stable at the time scale of the electrolysis experiment.

The TD-DFT UV–vis spectrum generated by the ADF code for the $MTAQ^{\bullet-}$ radical allows us to identify the main features of the experimental spectrum. We describe here only three, of all computed absorption bands, involving five molecular orbitals ADF-labelled # 57β (π-sulphur S), # 59α,β (π-S,O and C10 in standard nomenclature), # 60α (π-C1,4,5,8,9 carbon atoms) and # 61α (π-C2,3,4a,6,7,8a,9a,10a carbon atoms). These five orbitals have been computed with the ORCA package and drawn with the GopenMol software (Table S2). The absorption band computed at 527 nm (exp.) corresponds to a sulphur → sulphur charge transfer (CT; # 57β → # 59β), the band at 500 nm (exp.) to a sulphur → carbon CT (# 59α → # 61α) and the NIR-band at 852 nm (exp.) to a sulphur → carbon CT (# 59α → # 60α). Therefore, in general all of the main features of the experimental spectrum are reproduced by the TD-DFT calculations on the $MTAQ^{\bullet-}$ radical (Fig. S10).

The spectroelectrochemical studies together with the EPR experiments showed that $AQ^{\bullet-}$ and $MTAQ^{\bullet-}$ radicals are stable at electrolysis time scale and their oxidation processes are reversible. These results allow us to conclude that the decrease of the specific capacity of the MTAQ over the firsts 5 cycles is most certainly due to the dissolution of the active material into the electrolyte. Consequently the dissolved active materials diffuse to the lithium electrode and are reduced leading to their irreversible precipitation as lithium salts.

4. Conclusion

Our work presents for the first time a new quinone-based system for which one carbonyl function was replaced with a thiocarbonyl group. This compound was studied as an organic active material for lithium-ion batteries. Monothioanthraquinone showed better electrochemical performances compared to anthraquinone. First, the initial capacity is improved from 214 mAh g^{-1} to 222 mAh g^{-1}. In addition the higher potential of MTAQ is more appropriate for their use as active material for positive electrodes. Strong fundamental investigations were performed in order to better understand the electrochemical performances of this material by electrochemical, spectroelectrochemical, EPR studies and DFT calculations.

Finally, the present study revealed that the replacement of a carbonyl group with a thiocarbonyl was an effective way to improve the cycle-life stabilities and thoroughly adjust the working potential for the lithium complexation/decomplexation organic materials.

Acknowledgements

This work is part of METEOR project and was founded by the NTE program of the CEA.

Appendix A. Supplementary data

Supplementary data related to this article can be found at http://dx.doi.org/10.1016/j.jpowsour.2014.05.050.

References

[1] D.L. Williams, J.J. Byrne, J.S. Driscoll, J. Electrochem. Soc. 116 (1969) 2.
[2] P. Novák, K. Müller, K.S.V. Santhanam, O. Haas, Chem. Rev. 97 (1997) 207.
[3] Y. Liang, Z. Tao, J. Chen, Adv. Energy Mater. 2 (2012) 742.
[4] P.S. Guin, S. Das, P.C. Mandal, Int. J. Electrochem. 2011 (2011) 1.
[5] M. Armand, J.-M. Tarascon, Nature 451 (2008) 652.
[6] H. Chen, M. Armand, G. Demailly, F. Dolhem, P. Poizot, J.-M. Tarascon, ChemSusChem 1 (2008) 348.
[7] H. Chen, M. Armand, M. Courty, M. Jiang, C.P. Grey, F. Dolhem, J.-M. Tarascon, P. Poizot, J. Am. Chem. Soc. 131 (2009) 8984.
[8] M. Yao, S. Yamazaki, H. Senoh, T. Sakai, T. Kiyobayashi, Mater. Sci. Eng. B 177 (2012) 483.
[9] W. Wang, W. Xu, L. Cosimbescu, D. Choi, L. Li, Z. Yang, Chem. Commun. 48 (2012) 6669.
[10] Z. Lei, W. Wei-kun, An-bang Wang, Y. Zhong-bao, C. Shi, Y. Yu-sheng, J. Electrochem. Soc. 158 (2011) A991.
[11] L. Xie, L. Zhao, J. Wan, Z. Shao, F. Wang, S. Lv, J. Electrochem. Soc. 159 (2012) A499.
[12] P. Bu, S.Q. Liu, Y. Lu, S.X. Zhuang, H.Y. Wang, F.Y. Tu, Int. J. Electrochem. Sci. (2012) 4617.
[13] A.L.M. Reddy, S. Nagarajan, P. Chumyim, S.R. Gowda, P. Pradhan, S.R. Jadhav, M. Dubey, G. John, P.M. Ajayan, Sci. Rep. 2 (2012).
[14] R. Zeng, X. Li, Y. Qiu, W. Li, J. Yi, D. Lu, C. Tan, M. Xu, Electrochem. Commun. 12 (2010) 1253.
[15] Z. Song, H. Zhan, Y. Zhou, Chem. Commun. (2009) 448.
[16] W. Xu, A. Read, P.K. Koech, D. Hu, C. Wang, J. Xiao, A.B. Padmaperuma, G.L. Graff, J. Liu, J.-G. Zhang, J. Mater. Chem. 22 (2012) 4032.
[17] K. Oyaizu, W. Choi, H. Nishide, Polym. Adv. Technol. 22 (2011) 1242.
[18] K. Naoi, S. Suematsu, A. Manago, J. Electrochem. Soc. 147 (2000) 420.
[19] Y. Liang, P. Zhang, S. Yang, Z. Tao, J. Chen, Adv. Energy Mater. (2013) 600.
[20] M.S. Raasch, J. Org. Chem. 44 (1979) 632.
[21] Y.A. Jackson, D. Rajagopal, J. Bendolph, M. Guillory, M.V. Lakshmikantham, J. Yang, M.P. Cava, Org. Lett. 5 (2003) 1883.
[22] J. Moussa, D.A. Lev, K. Boubekeur, M.N. Rager, H. Amouri, Angew. Chem. Int. Ed. 45 (2006) 3854.
[23] M.V. Lakshmikantham, M. Levinson, M. Menachery, M.P. Cava, J. Org. Chem. 51 (1986) 411.
[24] H. Bock, S. Mohmand, T. Hirabayashi, G. Maier, H.P. Reisenauer, Chem. Ber. 116 (1983) 273.
[25] A. Levy, S. Pogodin, S. Cohen, I. Agranat, Eur. J. Org. Chem. 2007 (2007) 5198.
[26] S. Stoll, A. Schweiger, J. Magn. Reson. 178 (2006) 42.
[27] G. te Velde, E.J. Baerends, J. Comput. Phys. 99 (1992) 84.
[28] A.D. Becke, J. Chem. Phys. 98 (1993) 1372.
[29] C. Lee, W. Yang, R.G. Parr, Phys. Rev. B 37 (1988) 785.
[30] A. Klamt, G. Schüürmann, J. Chem. Soc. Perkin Trans. 2 (1993) 799.
[31] A. Klamt, J. Phys. Chem. 99 (1995) 2224.
[32] A. Klamt, V. Jonas, J. Chem. Phys. 105 (1996) 9972.
[33] F. Kootstra, P.L. de Boeij, J.G. Snijders, J. Chem. Phys. 112 (2000) 6517.
[34] P. Romaniello, P. de Boeij, Phys. Rev. B 71 (2005).
[35] O.V. Gritsenko, P.R.T. Schipper, E.J. Baerends, Chem. Phys. Lett. 302 (1999) 199.
[36] L. Palatinus, G. Chapuis, J. Appl. Crystallogr. 40 (2007) 786.
[37] O.V. Dolomanov, L.J. Bourhis, R.J. Gildea, J.A.K. Howard, H. Puschmann, J. Appl. Crystallogr. 42 (2009) 339.
[38] L.J. Farrugia, J. Appl. Crystallogr. 30 (1997) 565.
[39] A.J. Wain, G.G. Wildgoose, C.G.R. Heald, L. Jiang, T.G.J. Jones, R.G. Compton, J. Phys. Chem. B 109 (2005) 3971.
[40] A. Babaei, P.A. Connor, A.J. McQuillan, S. Umapathy, J. Chem. Educ. 74 (1997) 1200.
[41] T. Yamamoto, H. Etori, Macromolecules 28 (1995) 3371.
[42] M. Büschel, C. Stadler, C. Lambert, M. Beck, J. Daub, J. Electroanal. Chem. 484 (2000) 24.
[43] L.V. Natarajan, C. Lenoble, R.S. Becker, J. Phys. Chem. 91 (1987) 6606.
[44] A. Alberti, M. Benaglia, Gazz. Chim. Ital. 119 (1989) 537.
[45] C.O. Laoire, E. Plichta, M. Hendrickson, S. Mukerjee, K.M. Abraham, Electrochim. Acta 54 (2009) 6560.